Dynamic ice loads on conical structures

Yan Huang[a)] and Xuehua Li
School of Civil Engineering, Tianjin University, Tianjin 300072, China

(Received 30 November 2010; accepted 26 January 2011; published online 10 March 2011)

Abstract Two series of model tests were performed to observe the dynamic ice loads on conical structures. The variable testing parameters include the water line diameter of the model cone and ice parameters. During small water line diameter tests, two-time breaking is found to be the typical failure of ice on steep conical structure, and also be controlled by other factors, such as ice speed and the cone angle. During big water line diameter tests, the ice sheet failed nonsimultaneously around the cone. Several independent zones of bending were found in the nonsimultaneous failure process of ice. With the increase of the ratio of D/h and the number of independent zones, the total ice force was found being gradually reduced. [doi:10.1063/2.1102207]

Keywords conical structure, model test, ice load

In the designs of ocean engineering structures for cold region countries, ice loads are always one of the control loads, and the design of ice-resisting structures is one of the most important design aspects. Scale-model tests have verified that the ice force on a conical structure is significantly lower than that on a cylindrical structure of similar size.[1–5] As a result, conical structures are widely used in the design of ice-resisting structures, as the offshore wind turbine foundations in Denmark and oil platforms in the Bohai Bay.

However, the ice force is provided with periodic characteristic by the bending failure of ice sheet. To establish the numerical model of the dynamic ice loads on compliant conical structures, further research and improvements should be performed. From 2005 to 2009, the Ice Engineering Laboratory of Tianjin University started the model test study of the dynamic ice loads on conical structures. Some important findings will be discussed in this paper.

The tests were performed in the ice tank at the Ice Engineering Laboratory of Tianjin University.[6,7] The model ice was urea ice. "Wet seeding" with small ice crystals was used to start the ice sheet growth when the water and the ambient temperatures were 0 and −10°C, respectively. All of the ice crystal diameters were smaller than 1 mm, which satisfied the test requirements.

The first series of tests were performed with a compliance equipment to simulate flexural structure. The conical model was mounted to the compliance equipment through a load sensor, which is used to measure directly the ice force acting on the model, as shown in Fig. 1(a). By varying the vertical position of the model, two water line diameters of the cone were achieved, i.e. 0.2 m and 0.4 m. The cone angle is designed as 60°, which is the same as the cones on JZ20-2 platforms.

To investigate the influence of cone size on ice load, the second series of tests were performed with a conical model in big scale. The model cone consists of two parts, as shown in Fig. 1(b). The foundational part is a complete cone with 1.28 m bottom diameter and 0.2 m top diameter. To create serial independent measurement areas, a series of steel plates that are wedge shaped in length and arc shaped in width were installed from the front surface of the foundational cone. These plates which were equally cut from a whole cone form a new and bigger conical surface with 1.4 m bottom diameter and 0.22 m top diameter. Each plate was installed on the foundational cone through two load sensors, whose measuring capacity is 2 kN. The two load sensors were placed at top and bottom of the foundational cone, respectively. To ensure the independence of each measure area that includes one plate and two load sensors, the plates were arranged with a gap distance of 2 mm between each other. The ice load on each plate can be obtained by summing up the records captured from the corresponding load sensors. Five water line diameters (the diameters of the cone with the panels) were conducted in the tests: 0.4 m, 0.6 m, 0.8 m, 1.0 m and 1.2 m.

The ice sheet before the compliant cone was failed by two-time breaking in small scale tests. After the ice sheet was pushed up by the conical surface and broke abruptly, the wedge-shaped ice beams between the conical surface and intact ice sheet broke again at certain moment with the moving of carriage. After this second-time breaking, the climbing-cleaning process of the wedge blocks just started.

One typical ice force time-series indicating the two-time breaking events is shown in Fig. 2. To obtain the spectrum of the ice force, a fast Fourier transform is performed on the total ice force time-series, as shown in Fig. 2. Two distinct main frequencies exist in the figure, indicating that the wedge shaped ice beams broke again after the first breaking event initiated by initial circumferential cracks.

The shape of ice force acting on steep cone can be generally described by Fig. 3, in which F_1 is the ice force peak created by the first breaking, F_2 is the ice force peak created by the second-time breaking, F_3 is the

a)Corresponding author. E-mail: hjacyky@tju.edu.cn.

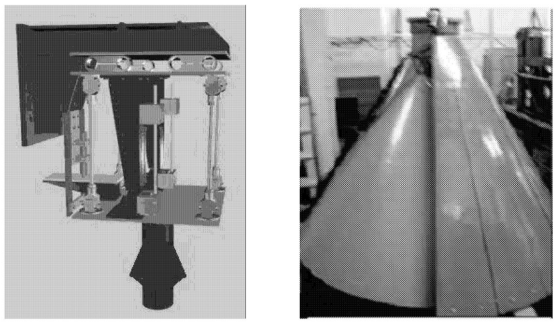

(a) (b)

Fig. 1. Pictures of the model cones

remanent ice force after the first unloading course and T is the whole period of the two-time breaking process. The ice force form can be described from the following aspects.

(1) General period T

T is determined by the break length l and ice speed V. As known, the break length is proportional to ice thickness h. By analyzing the test data, we found that this proportion is not a fixed value, but controlled by ice speeds. Introducing the dimensionless form of V, the relationship can be described as

$$l/h = 10.79 - 4.88V/\sqrt{gh}, \tag{1}$$

Four parameters t_1, t_2, t_3 and t_4 compose the general period, which is determined by l. Analyses results show that the proportions of these parameters are not influenced by the test conditions

$$\begin{aligned} &t_1/t_2 \approx 1.05, \quad t_3/t_4 \approx 0.98, \\ &T_1/T_2 = \frac{t_1 + t_2}{t_3 + t_4} \approx 1.25. \end{aligned} \tag{2}$$

(2) Acting level of the second breaking ice force

The acting level of the second breaking ice force, which determines the energy level of the high frequency component, is the most important parameter in the ice force function. One factor r that describes this level can be defined as

$$r = \frac{F_1 - F_3}{F_2 - F_3}. \tag{3}$$

This factor is also controlled by ice speed V

$$r = -0.33 + 0.97V/\sqrt{gh}. \tag{4}$$

(3) Remanent ice force level

The remanent ice force level indicates the beginning of the second breaking event and also reflects the correlation degree of the two breaking events. The remanent ice force level can be defined as F_3/F_1. Analyses results show that the factor is also controlled by ice speed V

$$F_3/F_1 = 0.97 - 0.89V/\sqrt{gh}. \tag{5}$$

Uncorrelated ice wedges occurred in most of the big scale tests. Decreased rubble piece sizes and disordered cracks in large water line diameter tests indicate that the ice sheet failed nonsimultaneously around the cone. Similar to the nonsimultaneous crushing failure of ice, there are several independent zones of bending during the ice failure process on wide conical structures. The radial cracks plot out these independent zones on the front of ice sheet, and the circumferential cracks start nonsimultaneously in these zones. However, different with the zones in nonsimultaneous crushing failure process, the zones in bending behave in a relatively stable manner. Such differences should arise from the different propagation modes of the cracks and the different breaking sizes of ice in bending and crushing failures.

To describe the problems concisely, here we choose one series of ice load records on 1# and 5# plates and the total ice force record to present the measured ice loads in the tests, as shown in Fig. 4.

The ice force time-series shown in Fig. 4 can also prove the existence of these independent zones of bending. The local ice loads on various measuring plates are different in both of phases and shapes. At the same time, each local ice force time-series still keeps most characteristics of the loads initiated by bending failure. So it indicates that the failures of ice sheet on these areas are nonsimultaneous and independent to each other.

In the tests, it was found that the number of independent zones depended on the ratio of D/h (D presents the water line diameter). When the ratio is below 20, the failures of ice wedges around the cone occur simultaneously. When $D/h > 25$, the failures of ice wedges around the cone start to behave nonsimultaneously. In the case of $25 < D/h < 30$, 3 to 4 independent zones were found in the tests. And 6 to 8 independent zones were found in the tests for $35 < D/h < 50$. In the tests with the biggest water line diameter ($D/h > 55$) of the cone, two or three independent zones occurred on one measuring area, and thus the number of independent zones is hard to be estimated.

The results of the two series of model tests indicate that the failing behavior of the ice wedges has remarkable influences on the ice loads. The maximum total ice force measurements for each test are presented in Fig. 5. The maximum total ice force occur in the case of $25 < D/h < 30$, with 3 to 4 independent zones existing in the bending failure process. The data indicates

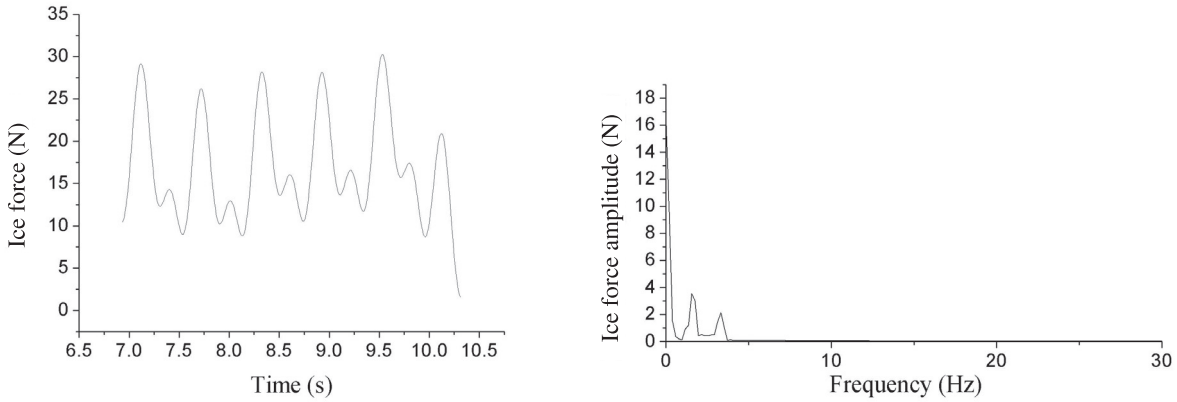

Fig. 2. Measured ice force data in small scale test and its spectrum

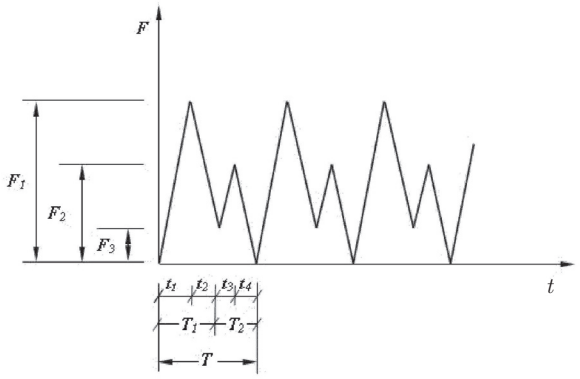

Fig. 3. Schematic diagram of the ice force function

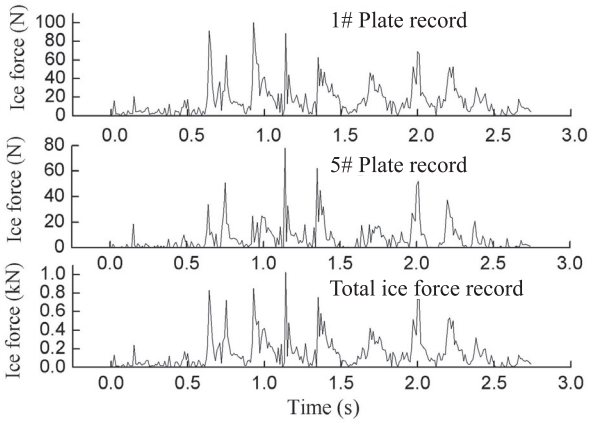

Fig. 4. Measured ice force data in big scale test

that the total ice load is increasing for lower D/h ratio, but reducing for higher D/h ratio and subsequent number of independent zones.

The work was supported by the National Natural Science Foundation of China (50609015).

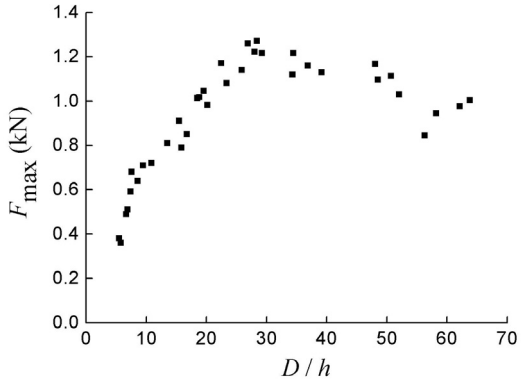

Fig. 5. Plotted results of $F_{\max}$ against D/h

1. T. Ralston, Proc. POAC 1977, Memorial University of Newfoundland, St. John's, Newfoundland, Canada, **2**:741 (1977).
2. K. Hirayama, and I. Obara, Proc. of the 5th International Offshore Mechanic Sand Arctic Engineering. Tokyo, Japan, 515 (1986).
3. M.B. Irani, and G. Timco, International Journal of Offshore and Polar Engineering, **3**, 313 (1993).
4. O. Pironneau, *Finite Element Methods for Fluids*, 2nd edn. (John Wiley and Sons, Chichester, 1989)
5. A. Barker, G. Timco, H. Gravesen, and P. Volund, Cold Regions Science and Technology **41**, 1 (2005).
6. Y. Huang, Q. Z. Shi, and A. Song, Cold Regions Science and Technology **49**, 151 (2007).
7. Y. Huang, Cold Regions Science and Technology **63**, 87 (2010).